Position and energy-resolved particle detection using phonon-mediated microwave kinetic inductance detectors

D.C. Moore,[1,a)] S.R. Golwala,[1] B. Bumble,[2] B. Cornell,[1] P.K. Day,[2] H.G. LeDuc,[2] and J. Zmuidzinas[1,2]
[1)] *Division of Physics, Mathematics & Astronomy, California Institute of Technology, Pasadena, CA 91125, USA*
[2)] *Jet Propulsion Laboratory, California Institute of Technology, Pasadena, CA 91109 USA*

We demonstrate position and energy-resolved phonon-mediated detection of particle interactions in a silicon substrate instrumented with an array of microwave kinetic inductance detectors (MKIDs). The relative magnitude and delay of the signal received in each sensor allows the location of the interaction to be determined with sub-mm precision. Using this position information, variations in the detector response with position can be removed, and an energy resolution of $\sigma_E = 0.55$ keV at 30 keV was measured. Since MKIDs can be fabricated from a single deposited film and are naturally multiplexed in the frequency domain, this technology can be extended to provide highly-pixelized athermal phonon sensors for ∼1 kg scale detector elements. Such high-resolution, massive particle detectors would be applicable to next-generation rare-event searches such as the direct detection of dark matter, neutrinoless double-beta decay, or coherent neutrino-nucleus scattering.

Next generation rare-event searches, such as the direct detection of dark matter[1], require large target masses ($\sim10^3$ kg) with sub-keV energy resolution. This requires increasing the mass of current solid-state, cryogenic experiments[2,3] by 2 orders of magnitude, while maintaining the background-free operation of existing detectors. Reducing the cost and time needed to fabricate and test each detector element is necessary for such large cryogenic experiments to be feasible.

Detectors that measure both the athermal phonons and ionization created by a particle interaction have demonstrated sufficient background rejection to enable next-generation experiments[4]. Microwave kinetic inductance detectors (MKIDs)[5,6] offer several advantages for providing athermal phonon sensors in large experiments relative to the transition edge sensor (TES)-based designs currently in use[2,7]. MKID-based phonon sensors can be patterned from a single deposited aluminum film, with large (>10 μm) features, significantly reducing fabrication time and complexity. Since MKIDs are naturally multiplexed in the frequency domain, hundreds of sensors can be read out on a single coaxial cable, enabling a more granular phonon sensor which is expected to provide enhanced background rejection. In addition to dark matter direct detection, high-resolution, massive particle detectors are applicable to the detection of neutrinoless double beta decay[8] and coherent neutrino-nucleus scattering[9].

In analogy to successful TES-based detectors[2], previous designs[10–12] attempted to absorb the incident energy in large area collectors that were coupled to smaller volume, distributed MKIDs. Although separating the absorber and sensor allowed increased sensitivity by concentrating the absorbed energy, test devices suffered from poor transmission of quasiparticles from the absorber to sensor. Here we present a simplified design that eliminates the absorber by directly collecting the energy using large-area MKIDs. A similar design developed independently by Swenson et. al.[13] has been used to demonstrate time-resolved phonon-mediated detection of high-energy interactions from cosmic rays and natural radioactivity using MKIDs. We have previously demonstrated energy-resolved detection of 30 keV x-rays[14] using phonon-mediated MKIDs fabricated from high-resistivity nitride films[15,16], but the energy resolution was limited to $\sigma_E = 1.2$ keV by systematic variations in the reconstructed energy with interaction location. In this work, we present results for devices fabricated from aluminum films that exhibit improved uniformity. These more uniform devices allow the location of the interaction to be determined and a position-based correction to be applied. This correction improves the resolution by more than a factor of 2 and recovers a reconstructed energy resolution within 40% of the baseline resolution.

To calculate the expected detector resolution, we assume that the phonons uniformly illuminate the substrate surface and that incident phonon energy is converted into quasiparticles in the inductive section of the resonators with overall efficiency η_{ph}. In this case, the phonon lifetime, τ_{ph}, is determined by the substrate geometry and fraction, η_{fill}, of the total surface area, A_{sub}, that is covered by MKIDs. To resolve the rising edge of the phonon signal requires that the quality factor $Q \leq 10^4$ for resonant frequencies $f_0 \approx 3$ GHz to give a resonator response time $\tau_{res} = Q/\pi f_0 \approx 1$ μs. For $\eta_{fill} \approx 5\%$ as in existing TES-based designs[4], $\tau_{ph} \approx 1$ ms, while quasiparticle lifetimes, τ_{qp}, in our films are measured to be 10–100 μs. Given these characteristic times, we assume $\tau_{res} \ll \tau_{qp} \ll \tau_{ph}$. The resonator quality factor, $Q^{-1} = Q_c^{-1} + Q_i^{-1}$, depends on both the coupling quality factor, Q_c, due to energy losses through the coupling capacitor and the internal quality factor, Q_i, due to all other losses in the resonator (e.g., dissipation due to quasiparticles). For our devices, typically $Q_i > 10^6$, so $Q_c \ll Q_i$ is required for sufficient sensor bandwidth to resolve the phonon rise time. At low temperatures, the steady-state quasiparticle number is dominated by quasiparticles generated by readout power[17], P_{read}, and

a) Electronic mail: davidm@caltech.edu

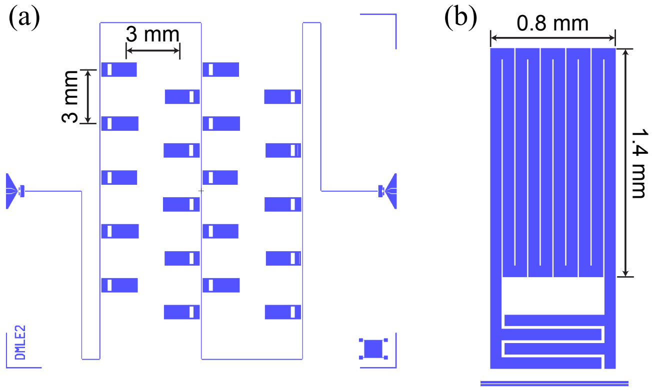

FIG. 1. (a) Array layout. The resonators are arranged in an offset grid with 3 mm spacing between the neighboring rows and columns and are coupled to a coplanar strip feedline. (b) Resonator geometry. Each resonator consists of a meandered inductor connected to an interdigitated capacitor, with total inductor area ≈1 mm^2.

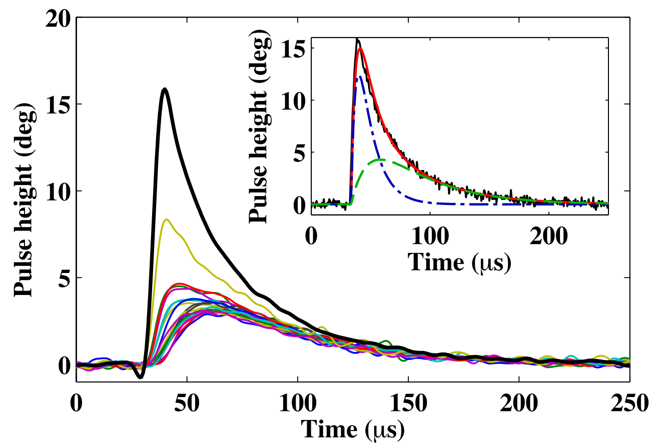

FIG. 2. (Color online) Example pulses observed in each resonator for a 200 keV energy deposition. The pulse heights have been rescaled by each resonator's relative responsivity, and a 200 kHz low-pass filter has been applied. The resonator closest to the interaction site has a large, prompt response (thick, black), while the resonators farther from the interaction have smaller, delayed responses. (inset) Two-template optimal filter fit (red, solid) to the pulse in the primary channel. The pulse contains a prompt component (blue, dash-dotted) that decays away with the quasiparticle lifetime as well as a delayed component (green, dashed) that decays away with the phonon lifetime.

$N_{qp} = \eta_{read} P_{read} \tau_{qp}/\Delta$, where Δ is the superconducting gap and $\eta_{read} \leq 1$ is the efficiency for the readout power to create quasiparticles in the resonator. Finally, we assume that frequency-based readout is used with the noise at the signal frequencies of interest dominated by the HEMT amplifier with noise temperature, T_N.

Given these assumptions, the expected energy resolution for an MKID-based phonon-mediated detector is[6,14]:

$$\sigma_E = \frac{\Delta}{\eta_{ph}\beta(\omega,T)} \sqrt{\frac{\eta_{read}}{\alpha p_t} \frac{A_{sub} k_b T_N}{2\pi f_0} \frac{N_0 \lambda_{pb}}{\tau_{qp} S_1(\omega,T)}} \quad (1)$$

where p_t is the probability for a phonon to be transmitted from the substrate to the MKID, α is the fraction of the total inductance of the resonators due to kinetic inductance, and λ_{pb} is the characteristic pair-breaking length in the MKID[18]. The ratio of the frequency to dissipation response is defined as $\beta = S_2/S_1$, where $S_1(\omega,T)$ and $S_2(\omega,T)$ are dimensionless factors of order unity given by Mattis-Bardeen theory[19,20].

To demonstrate the detection principle and verify the sensitivity calculation in Eq. 1, prototype arrays of 20 resonators were designed. Fabrication constraints limited the substrate dimensions to 22 mm x 20 mm. Twenty resonators with inductor area A_{ind} = 1 mm^2 were arranged in a grid, as shown in Fig. 1a. The resonator design, shown in Fig. 1b, consisted of a lumped-element geometry[21] with a 70 μm wide meandered inductor connected to an interdigitated capacitor with 20 μm spacing between fingers. The resonant frequencies were evenly spaced by 10 MHz so that the entire array fit within 200 MHz of bandwidth around 4.8 GHz.

Devices were fabricated on 1 mm thick, high-resistivity Si substrates ($\rho \geq 5$ kΩ cm), which were deglazed in dilute hydrofluoric acid (HF) just prior to vacuum processing. The resonators were patterned by inductively coupled plasma etching (BCl_3/Cl_2) of a single, 25 nm thick aluminum film deposited by dc magnetron sputtering at ambient temperature. The substrates were mounted to a testing enclosure with GE varnish at the corners of the chip, with total contact area of 8 mm^2. An ^{129}I source was mounted to illuminate the substrate face opposite the resonators, and the enclosure was cooled to 50 mK in a dilution refrigerator.

Figure 2 shows the phase response for each of the 20 resonators following an example 200 keV interaction in the substrate from a cosmic-ray or natural radioactivity. The location of the interaction can be determined by the relative partitioning of the energy between the resonators and the timing of the response seen in each channel[13,22].

The measured coupling Q varied from 5×10^3–5×10^4, leading to a corresponding variation in the responsivity of each channel. The relative responsivity was calibrated using events depositing >500 keV by matching the exponential tails of the pulses after the initial position-dependent information had decayed away[4]. After calibrating for the responsivity, we denote the "primary channel" as the resonator showing the largest response, and the "opposite channels" as the group of resonators showing the smallest, position-independent response.

As shown in Fig. 2, the pulse shape varies significantly between the primary and opposite channels. We find that the measured pulses, $p(t)$, are well described by the sum of two components plus a noise term: $p(t) = A_p s_p(t) + A_o s_o(t) + n(t)$, where A_p is the amplitude of the prompt component of the pulse that decays with the quasiparticle lifetime, A_o is the amplitude of the delayed component of the pulse that decays with the phonon lifetime and $n(t)$ is a noise realization. The pulse shape for the prompt component and delayed component is given by s_p and s_o, respectively. These templates are determined by first averaging many opposite channel pulses and fitting to a double-exponential functional form to determine s_o. The prompt template, s_p, is then determined by fitting an averaged primary channel pulse to a model with a fixed component equal to s_o plus an additional double-exponential form. The standard optimal filter formalism then gives the amplitude estimates for each pulse component for the ith channel as:

$$\begin{pmatrix} \hat{A}_{p,i} \\ \hat{A}_{o,i} \end{pmatrix} = M^{-1} \begin{pmatrix} \sum \mathrm{Re}\left(\tilde{s}_p^* \tilde{p}_i\right) J^{-1} \\ \sum \mathrm{Re}\left(\tilde{s}_o^* \tilde{p}_i\right) J^{-1} \end{pmatrix} \tag{2}$$

where the sum runs over the length of the trace, $\tilde{s}_{p,o}$ and $\tilde{p}_i$ denote the Fourier transforms of $s_{p,o}$ and p_i, J is the power spectral density of the noise and:

$$M = \begin{pmatrix} \sum |\tilde{s}_p|^2 J^{-1} & \sum \mathrm{Re}(\tilde{s}_p^* \tilde{s}_o) J^{-1} \\ \sum \mathrm{Re}(\tilde{s}_p^* \tilde{s}_o) J^{-1} & \sum |\tilde{s}_o|^2 J^{-1} \end{pmatrix} \tag{3}$$

An example optimal filter fit to the primary pulse for a 200 keV event is shown in the inset of Fig. 2.

The energy of the pulse is then reconstructed from the optimal filter amplitudes as $E = E_0 \sum_i (\hat{A}_{p,i} + w\hat{A}_{o,i})/r_i$, where the latter component is weighted by the ratio of the template integrals, $w = \sum s_o / \sum s_p$, and the index i runs over the resonators in the array. Since the two pulse components measure the quasiparticle creation rate in the prompt and slow components convolved with the quasiparticle decay time, w gives the ratio of the total number of quasiparticles created in these components, noting that the linear convolution does not affect the ratio. The relative responsivity of each resonator is given by r_i while the overall scaling, E_0, is determined by calibration with x-ray lines of known energy. Figure 3 shows the reconstructed energy spectrum for phonon-mediated events from an ^{129}I source.

The frequency and dissipation response of the resonators with temperature was used to determine $\alpha = 0.075 \pm 0.005$ and $\Delta = 204 \pm 21$ μeV from fits to Mattis-Bardeen theory[19]. Comparing the phase response versus temperature to the phase response for events from the source indicates that $\eta_{ph} = 0.070 \pm 0.011$. Measurements of the frequency noise confirm that the measured noise is consistent with HEMT noise for $T_N = 5$ K. The quasiparticle lifetime, $\tau_{qp} = 12.9 \pm 1.2$ μs, was determined from the fall time of the prompt component of the primary channel pulses. Using these parameters and Eq. 1, the expected resolution for this device was σ_E=(0.48 keV)$\sqrt{\eta_{read}/p_t}$, consistent with the measured baseline resolution for $\sqrt{\eta_{read}/p_t} \approx 0.8$.

Although the baseline resolution is consistent with expectations, the measured energy resolution at 30 keV is $\sigma_E \approx 1$ keV. This is a factor of 2.5 larger than the baseline resolution, indicating that systematic variations in the pulse shape or amplitude with position are dominating the resolution. In addition, non-Gaussian tails of events lie between the expected spectral peaks. To remove poorly collected events and account for these systematic variations, a simple position estimator was constructed from the relative partitioning of energy between sensors for each event[2,22]. For i resonators at locations (x_i,y_i) with energy E_i detected in each resonator, the "X energy partition" is defined as $P_x = \sum_i x_i E_i / \sum_i E_i$, and correspondingly for Y. Figure 4 shows the reconstructed event location using this position estimator. Although the relative timing of the signal can also be used to provide an independent determination of the event location, for this work we used only the partition information due to its higher signal-to-noise at 30 keV.

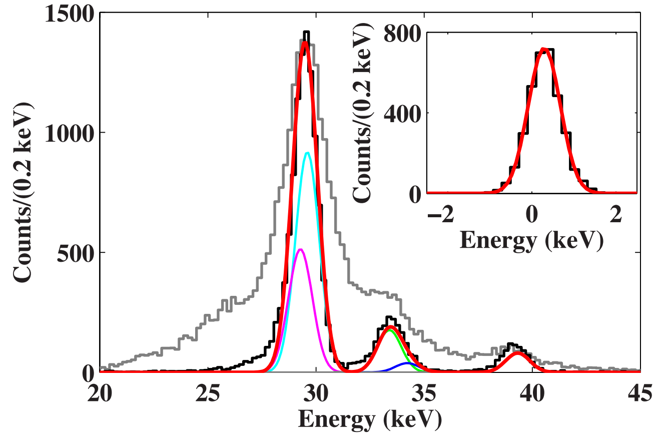

FIG. 3. (Color online) Observed spectrum when the substrate face opposite the resonators is illuminated with an ^{129}I source. The light histogram shows the reconstructed energy for all events prior to correcting for position-dependent smearing of the response. The dark histogram shows the spectrum after restricting to events interacting in the central portion of the substrate and applying a position-based correction to the energy. The spectrum is fit to the observed lines at 29.5 (29.8%), 29.8 (53.1%), 33.6 (10.2%), 34.4 (2.2%), and 39.6 keV (4.6%), where the numbers in parentheses denote the expected absorbed intensities in 1 mm of Si. The thick, red line shows the fit to the total spectrum, where only a single amplitude, mean and resolution are fit and the relative line positions and amplitudes are fixed to the known values above. The best fit resolution at 30 keV is $\sigma_E = 0.55$ keV. (inset) Fit to the reconstructed energy spectrum for randomly triggered noise traces. The inferred baseline resolution is $\sigma_E = 0.38$ keV.

For interactions occurring near the edge of the substrate, more phonon energy can be lost to the detector housing than for interactions in the center. Figure 4 shows a position-based selection of events that removes edge events with poor collection, eliminating nearly all of the events in the non-Gaussian tails between peaks.

In addition, a position-dependent correction for variations in the reconstructed energy was applied, similar to

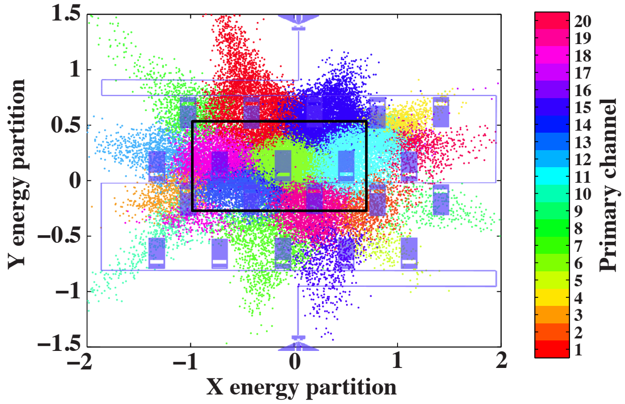

FIG. 4. (Color online) Reconstruction of the interaction location from the partitioning of energy between resonators. The coloring denotes the primary channel for each pulse. The black lines indicate the selection of events interacting in the center of the substrate. For comparison, the device geometry from Fig. 1 is overlaid.

the correction used in existing TES-based detectors[2,22]. For each event with energy partition location (P_x,P_y), the set of $n = 400$ events with the closest partition location were selected as a sample of events occurring physically close to the event under consideration. The spectrum for these "nearest neighbor" events was fit to determine the location of the 29.8 keV peak, and a correction was applied to the event in question to normalize its energy by the energy reconstructed for its nearest neighbors, $E^{corr} = (29.8\text{ keV}/E^{nn}_{29.8})E$, where E^{corr} is the position-corrected energy estimate and $E^{nn}_{29.8}$ is the location of the peak maximum for the event's nearest neighbors. The resulting spectrum is shown in Fig. 3. The best-fit resolution is $\sigma_E(30\text{ keV}) = 0.55$ keV. This resolution is nearly a factor of 2 better than the uncorrected resolution for all events and is within 40% of the baseline resolution of $\sigma_E(0\text{ keV}) = 0.38$ keV.

We are currently scaling this design to 0.25 kg substrates with $A_{sub} \approx 100$ cm^2. Existing TES-based phonon-mediated detectors of this size have typical energy resolutions[2] $\sigma_E = 1.0$ keV at 20 keV, indicating that the devices presented above can already provide comparable energy resolution. The energy resolution of MKID-based devices can also be significantly improved. Increasing the phonon collection efficiency to $\eta_{ph} = 30\%$, as obtained for TES-based designs with comparable metal coverage[4], would improve the resolution by a factor of 4. Using resonator materials with higher kinetic inductance or lower gap could also improve the resolution, provided uniform resonators can be fabricated. Finally, current devices are limited by amplifier noise, so the development of lower-noise, broadband amplifiers[23], could provide up to an additional factor of 3 improvement in resolution. At the same time, MKIDs would provide less complex detector fabrication and higher resolution position information to enhance background rejection, simplifying the extension of these designs to the large target masses needed for future rare-event searches.

This research was carried out in part at the Jet Propulsion Laboratory (JPL), California Institute of Technology, under a contract with the National Aeronautics and Space Administration. The devices used in this work were fabricated at the JPL Microdevices Laboratory. We gratefully acknowledge support from the Gordon and Betty Moore Foundation. This work benefited significantly from interactions with and simulation software developed by the CDMS/SuperCDMS collaborations, as well as from useful insights from B. Mazin and O. Noroozian. B. Cornell has been partially supported by a NASA Space Technology Research Fellowship.

[1] R. J. Gaitskell, Ann. Rev. Nucl. Part. Sci. **54**, 315 (2004).
[2] Z. Ahmed *et al.* (CDMS-II), Science **327**, 1619 (2010); G. Angloher *et al.* (CRESST-II), arXiv:1109.0702v1 (2011).
[3] E. Armengaud *et al.* (EDELWEISS-II), Phys. Lett. B **702**, 329 (2011).
[4] M. Pyle, B. Serfass, P. L. Brink, B. Cabrera, M. Cherry, N. Mirabolfathi, L. Novak, B. Sadoulet, D. Seitz, K. M. Sundqvist, A. Tomada, J. J. Yen, and B. A. Young, AIP Conf. Proc. **1185**, 223 (2009).
[5] P. K. Day, H. G. LeDuc, B. A. Mazin, A. Vayonakis, and J. Zmuidzinas, Nature **425**, 817 (2003).
[6] J. Zmuidzinas, Ann. Rev. Cond. Matt. Phys. **3**, 169 (2012).
[7] K. Irwin and G. Hilton, in *Cryogenic Particle Detection*, Topics in Applied Physics, Vol. 99, edited by C. Enss (2005) pp. 81–97.
[8] F. T. Avignone, III, S. R. Elliott, and J. Engel, Rev. Mod. Phys. **80**, 481 (2008).
[9] D. Z. Freedman, Phys. Rev. D **9**, 1389 (1974).
[10] D. C. Moore, B. A. Mazin, S. Golwala, B. Bumble, J. Gao, B. A. Young, S. McHugh, P. K. Day, H. G. Leduc, and J. Zmuidzinas, AIP Conf. Proc. **1185**, 168 (2009).
[11] S. Golwala, J. Gao, D. Moore, B. Mazin, M. Eckart, B. Bumble, P. Day, H. G. Leduc, and J. Zmuidzinas, J. Low Temp. Phys. **151**, 550 (2008).
[12] B. A. Mazin, B. Bumble, P. K. Day, M. E. Eckart, S. Golwala, J. Zmuidzinas, and F. A. Harrison, Appl. Phys. Lett. **89**, 222507 (2006).
[13] L. J. Swenson, A. Cruciani, A. Benoit, M. Roesch, C. S. Yung, A. Bideaud, and A. Monfardini, Appl. Phys. Lett. **96**, 263511 (2010).
[14] D. Moore, S. Golwala, B. Bumble, B. Cornell, B. Mazin, J. Gao, P. Day, H. LeDuc, and J. Zmuidzinas, J. Low Temp. Phys., *in publication* (2011), DOI:10.1007/s10909-011-0434-1.
[15] H. G. Leduc, B. Bumble, P. K. Day, B. H. Eom, J. Gao, S. Golwala, B. A. Mazin, S. McHugh, A. Merrill, D. C. Moore, O. Noroozian, A. D. Turner, and J. Zmuidzinas, Appl. Phys. Lett. **97**, 102509 (2010), arXiv:1003.5584.
[16] R. Barends, H. L. Hortensius, T. Zijlstra, J. J. A. Baselmans, S. J. C. Yates, J. R. Gao, and T. M. Klapwijk, Appl. Phys. Lett. **92**, 223502 (2008).
[17] P. de Visser, J. Baselmans, S. Yates, P. Diener, A. Endo, and T. Klapwijk, (2012), arXiv:1202.0816v1.
[18] S. B. Kaplan, C. C. Chi, D. N. Langenberg, J. J. Chang, S. Jafarey, and D. J. Scalapino, Phys. Rev. B **14**, 4854 (1976); A. Mrzyglod and O. Weis, J. Low Temp. Phys. **97**, 275 (1994); A. R. Long, J. Phys. F: Metal Phys. **3**, 2023 (1973).
[19] D. C. Mattis and J. Bardeen, Phys. Rev. **111**, 412 (1958).
[20] J. Gao, PhD thesis, California Institute of Technology (2008).
[21] S. Doyle, P. Mauskopf, J. Naylon, A. Porch, and C. Duncombe, J. Low Temp. Phys. **151**, 530 (2008).
[22] D. S. Akerib *et al.* (CDMS), Phys. Rev. D **72**, 052009 (2005).
[23] B. H. Eom, P. K. Day, H. G. Leduc, and J. Zmuidzinas, arXiv:1201.2392v1 (2012).